Diverse Morphologies of PVDF Hollow Fiber Membranes and Their Performance Analysis as Gas/liquid Contactors

Chunsheng Feng,[1] Rong Wang,[1,2,3] Hongyan Zhang,[1] Lei Shi[2]

[1]*School of Civil and Environmental Engineering, Nanyang Technological University, Singapore 639798*
[2]*Singapore Membrane Technology Centre, Nanyang Technological University, Singapore 639798*
[3]*Institute of Environmental Science and Engineering, Nanyang Technological University, Singapore 639798*

Received 1 June 2007; accepted 6 February 2009
DOI 10.1002/app.30250
Published online 18 August 2010 in Wiley Online Library (wileyonlinelibrary.com).

ABSTRACT: A systematic investigation on the morphology development of polyvinylidene fluoride hollow fiber membrane made using various *N*-methyl-2-pyrrolidone (NMP) aqueous solutions as an inner coagulant was carried out. The cross-sectional and inner surface morphology were analyzed with scanning electronic microscopy (SEM). It is found that with increase on NMP concentration, the morphology of the resultant membranes gradually shifted from a double-skin to a single-skin structure. When 40.0 $\sim$ 55.0 wt.% NMP solution was used, some unexpected macrovoids near the inner region were observed. This special morphology feature was attributed to the reduced solidification rate of the inner surface as a result of increase on NMP concentration, which sharply weakened the inner skin strength. While the existence of centralized stress formed in the phase inversion process, such as shrinkage stress from syneresis, resulted in fractured points in the nascent skin surface that finally made it difficult to maintain a uniform structure. Investigations on effects of the dope flow rate and the bore fluid velocity on the morphology of PVDF fiber membranes experimentally confirmed the suggestion. Three model membranes with double skins, single skin and single skin with macrovoids structures, respectively, were used to test their permeation performance in a CO_2 membrane contactor system. The experimental results show the membranes without an inner skin present higher permeability and lower mass transfer resistance than the membrane with a double skin structure. © 2010 Wiley Periodicals, Inc. Journal of Applied Polymer Science 119: 1259–1267, 2011

Key words: single skin; PVDF membrane; phase inversion; macrovoid; CO_2 capture

INTRODUCTION

Microporous hollow fiber membranes used in gas absorption or other stripping processes have attracted considerable attention since 1980s.[1–4] Hydrophobic polymers are preferential candidate materials for making membranes used as gas/liquid contactors, as hydrophobic nature of the membrane surface tends to repel aqueous droplets into the membrane pores to avoid a significant increase of mass transfer resistance.[5–7] Strong hydrophobic membranes such as polytetrafluoroethylene (PTFE) and polypropylene (PP) are commercially available and have been widely applied in laboratories or pilot scale set-up.[8,9] Another popular hydrophobic membrane material is polyvinylidene fluoride (PVDF), which is often grouped with PTFE and PP into one category. Unlike PTFE and PP, PVDF can be dissolved in common solvents such as NMP, N,N-dimethylacetamide (DMAc). As a result, most of PVDF membranes were manufactured via nonsolvent induced phase separation (NIPS) process, which is a relatively simple approach and can be performed in most of laboratories. Investigations on the preparation, morphology, and performance of PVDF hollow fiber membranes have been carried out extensively.[10–13]

The hollow fiber membranes formed by NIPS usually present an asymmetric structure, which consists of a selective (skin) layer and a porous sublayer. The selective layer keeps a high rejection and simultaneously imposes most of mass transfer resistance, whereas the sublayer usually provides a strong support for its porous structure. The current double-skin fiber membrane is often applied in liquid/liquid membrane contactor system, whereas the single-skin fiber membrane seems to be more advantageous in the gas absorption processes.[13]

The single-skin hollow fiber membrane is often prepared by two methods. One method is surface coating for high selective and permeable materials on a porous supporting substrate, which simplifies spinning operations and favorably strengthens mechanical performance of the composite membrane, but the leakage risk of the feed stream may rise if uneven surface coating is operated.

The other method is derived from NIPS, where a poor coagulant replaces a strong one as the inner or external coagulant. The formation approach does not

Correspondence to: R. Wang (rwang@ntu.edu.sg).

introduce any especial device except for changing the coagulant nature, therefore, it furthest succeeds the facility and flexibility in usual preparation of double-skin membranes. Many researchers have studied the effect of the inner or external coagulant on the structure and performance of hollow fiber membranes. Wijmans et al.[14,15] early noticed the effect of coagulants containing organic solvents on the membrane surface morphology. Fujii et al.[16] prepared PVDF hollow fiber membranes with high permeability by using a 80% DMSO aqueous solution as the injected coagulant. Deshmukh et al.[17] investigated the effect of ethanol/water composition as the external coagulant on the morphology of PVDF fiber membranes, but the investigation was ended at 50% ethanol content due to the difficulty encountered on preparing the membrane. Wang et al.[12] used ethanol as an inner coagulant to form PVDF fiber membranes with free-inner skin. Khayet et al.[18] made a comparative study on the change of pore size of PVDF hollow fiber membranes by introducing a 50% ethanol solution and water as the inner coagulant, respectively. Ren et al.[13] newly formed fine porous fiber membranes by employing a 85% NMP aqueous solution as the injected solution. A survey on relevant reports showed that a comprehensive effect of organic solutions with wide concentration ranges as the coagulant on PVDF fiber morphology has been rarely discussed, in particular, the transition morphology of the fiber membrane between the double skin and single skin hasn't been investigated as yet.

In this work, the wet-spinning process was purposely chosen to fabricate PVDF hollow fiber membranes, i.e., no air gap, consequently, the effects of the bore fluid and orientation induced within the spinneret on the membrane morphology could be saved adequately in spun fibers. A model system, PVDF/NMP/H_2O, was used to track the morphology development of PVDF membranes under different fabrication conditions. The formation mechanisms on diverse morphologies of the resultant membrane were tentatively analyzed. The mass transfer performance of the resultant membranes with typical structures was finally tested by a CO_2 absorption system.

EXPERIMENTAL

Membrane material and chemicals

PVDF (Kynar 740, pellet form) was supplied by Elf Autochem (USA). NMP (>99.5%) as a solvent was purchased from Merck. Some dextran $(C_6H_{10}O_5)_n$ samples with different molecular weights (1500–100,000; from Fluka) were used to characterize the molecular weight cut-off (MWCO) of hollow fiber membranes. Distilled water was used as a pore former, while tape water at 25°C was constantly used as an external coagulant throughout all the experiments. All the reagents were used as received.

Formation of PVDF hollow fiber membranes

The PVDF pellet, NMP and distilled water were mixed at 60°C under agitation for 7 days until a homogenous and stable solution was formed. The resulting solution was filtered to remove remnant contaminants, then, degassed about 24 h at room temperature. The dope after treatment was transferred into a stainless steel container that was connected with a N_2 gas cylinder. Under a certain pressure depending upon the requirement on the dope flow rate, the dope was extruded out the spinneret, and immediately immersed into the external precipitating bath (tape water). Various NMP aqueous solutions ranging from 0 to 90.0 wt % were respectively used as the bore fluid. To effectively prevent the nascent membrane from shrinkage in the following drying process, the hollow fiber membranes were immersed in turn into water/ethanol (1 : 1), pure ethanol over 24 h. The membranes were subsequently dried at room temperature before characterization tests.

Determination of water permeation flux and MWCO

Small test modules were made with 20 pieces of fiber membranes in a glass tube with an effective length of 27 cm. The membrane pore size was characterized based on the filtration of a dextran solution through gel permeation chromatography (GPC) on a Waters chromatography system (the ultrahydrogel columns 120, 250, 500). The water permeation flux was calculated according to water volume collected in unit time and surface area under 1bar pressure.

Test on CO_2 absorption of resultant membranes used as contactors

20 pieces of resultant membranes were encapsulated into a model module for CO_2 absorption test. Pure CO_2 was used as the feed gas while the N_2 saturated distilled water was used as the absorbent. The liquid passed through the shell-side and the gas flowed counter-currently through the lumen side of the hollow fibers, as the selective layers of PVDF hollow fibers were in the outer surfaces. The detailed experimental setup and test procedures could be found elsewhere.[19]

In CO_2 absorption experiments, overall mass transfer coefficient and mass transfer resistance was chosen to characterize the effect of various fibers structure on permeation performance. The overall mass transfer coefficient, K_{ol}, can be calculated based on experiments

by the following equation:

$$K_{ol} = \frac{Q_l(C_{l,out} - C_{l,in})}{A_T \Delta C_{l,av}} \quad (1)$$

The logarithmic mean concentration, $\Delta C_{l,av}$, is expressed as

$$\Delta C_{l,av} = \frac{(HC_{g,in} - C_{l,out}) - (HC_{g,out} - C_{l,in})}{\ln\left(\frac{HC_{g,in} - C_{l,out}}{HC_{g,out} - C_{l,in}}\right)} \quad (2)$$

where A_T is the gas–liquid contact area, $C_{l,in}$, $C_{l,out}$ are liquid phase inlet and outlet concentrations, $C_{g,in}$, $C_{g,out}$ are gas phase inlet and outlet concentrations, H is the Henry's constant, Q_l is the liquid volumetric flow rate. The particulars on above two equations can be referenced in Ref. 19 and 20.

Examination of the fiber membrane morphology

The dried membrane samples were broken in liquid nitrogen for the observation of the cross-section, while the dissection of the sample with a double-edge blade was used to examine inner surface morphology. The membrane samples were sputtered with a thin layer of gold using a SPI-Module sputter coater. The cross-section and inner surface of hollow fiber membranes were observed using a JEOL JSM-5310LV Scanning Electron Microscope (SEM).

RESULTS AND DISCUSSIONS

To decouple the effects of the dope component and external membrane formation situations on the membrane morphology, the dope composition and external precipitating bath were kept constant throughout the investigation. Table I lists the general spinning conditions of the model membranes.

TABLE I
Spinning Conditions of Model Membranes

Dope Solution Composition	PVDF/NMP/Distilled Water (17/80/3)
Dope flow rate (cm^3/min)	Varied
Bore fluid flow rate (cm^3/min)	Varied
Bore fluid composition	Distilled water or NMP aqueous solution
Air gap distance (mm)	0 (wetting spun)
External coagulant	tape water
Coagulant temperature (°C)	25
Dimensions of spinneret (mm/mm)	ID/OD (1.10/2.0)
Spinneret temperature (°C)	25
Room temperature (°C)	25
Room relative humidity (%)	60
Power-law equation[a]	$\tau = 1.482\ \gamma^{0.962}$

[a] Test at 25°C.

Diverse morphologies of PVDF fiber membranes from various bore fluids

Figure1 shows diverse morphologies of PVDF fiber membranes when various NMP aqueous solutions as an inner coagulant were pumped into the spinneret lumen. It can be seen that, with increase on NMP content in the inner coagulant, the cross-section morphologies of the fiber membranes gradually transferred from obvious double-skin [Fig. 1(A,B)] to single-skin structure [Fig. 1(C,D)], this is, a dense inner skin gradually developed into a porous inner surface [Fig. 1(a–d). The tendency seems to meet the argument of Wijmans et al.[14,15] However, the shifting course on the morphology, especially for the areas near the inner surface, didn't follow the trend at all times. As shown in Figure 2, when NMP solutions with a medium concentration, such as 40.0, 45.0, 50.0 and 55.0 wt %, were respectively used as an internal coagulant, the deformations of the inner fiber, especially the inner surface, were unexpectedly exhibited. Some macrovoids close to the inner surface deformed the original excellent circle shape although the size of macrovoids was gradually shrunk with increasing NMP concentration.

The development of the porous membrane structure is governed by complicated thermodynamic and kinetic factors. Any change from the spinning dope compositions and operating conditions generally imposes some effects on the final membrane morphology. In a wetting spin process, when a spinning dope was extruded out the spinneret, two couple mass transfers, the inner coagulant and the dope, and the outer coagulant and the dope, almost simultaneously took place, which cooperatively formed the final membrane morphology. When distilled water or a lower content NMP solution was used as the inner coagulant, the inner layer can be rapidly vitrified into a relative dense nascent skin. The rapid formation of the dense inner skin imposes a similar effect on the mass transfer of the inner sublayer as that of the outer skin, consequently, resulting in a similar structure with the outer sublayer. In addition, the vitrified nascent inner skin was strong enough to withstand unequilibrious stresses generated in the inner skin formation, such as shrinkage stress from syneresis,[21,22] to maintain an excellent circular shape in the cross section accordingly. However, with a further increase of NMP content in the bore fluid, such as from 40.0 to 55.0 wt %, the solidification rate of the inner surface gradually decreased, and the inner surface pore size gradually increased. The inner skin might became too weak to stand against the syneresis shrinkage and other uneven stresses beneath the surface, even resulted in an appearance of some fractured points, which possibly induced sharp mass transfer, finally leaded to the formation of some macrovoids or merger of adjacent pores in the inner sublayer. The nascent fibers were unable to self-support to maintain

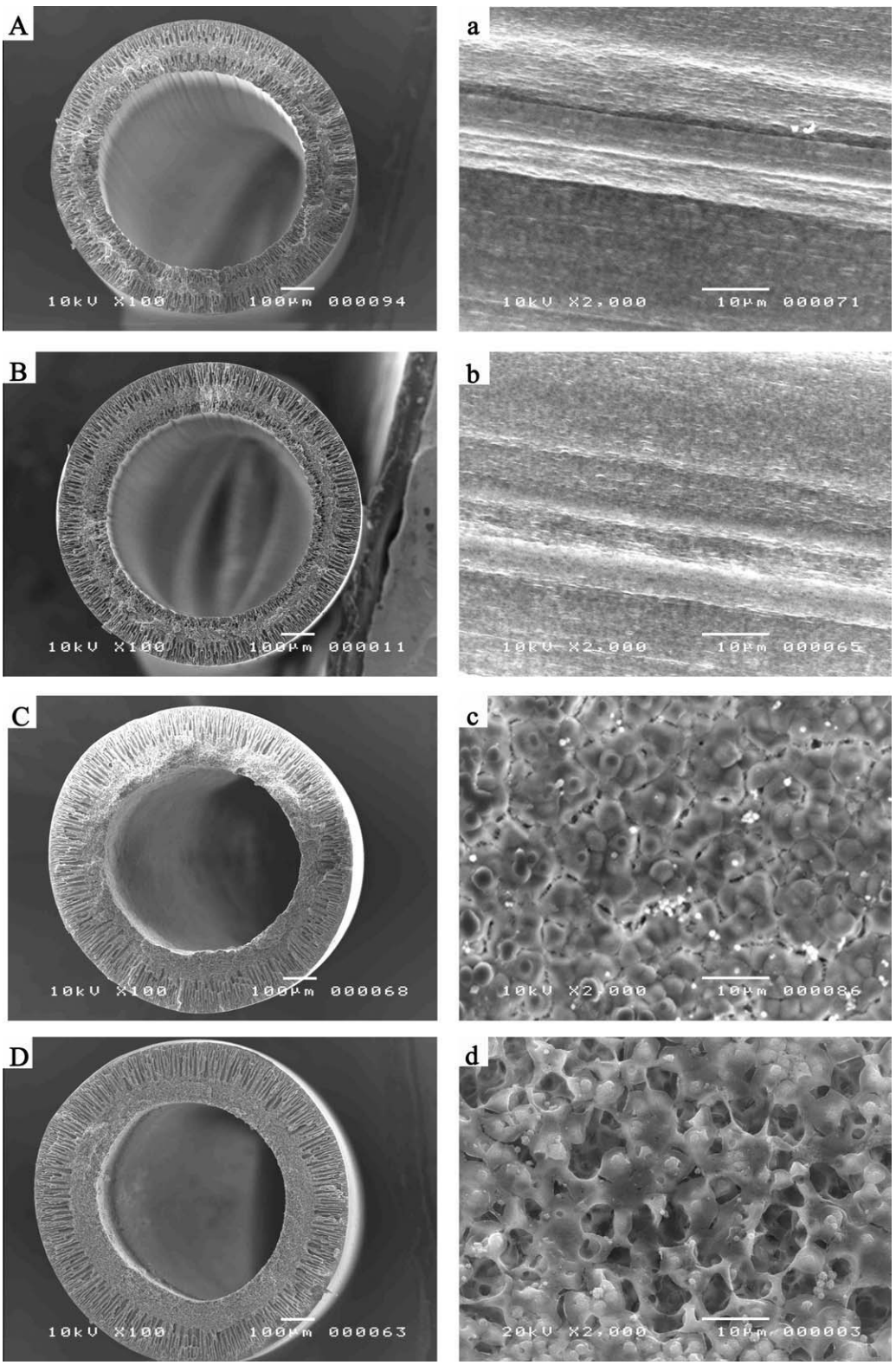

Figure 1 Cross-section and inner surface of hollow fiber membranes from various bore fluids. Dope flow rate, 12.14 cm^3/min; bore fluid rate, 4.0 cm^3/min; Inner coagulant, NMP aqueous solution. A, a: 0 wt%; B, b: 20.0 wt%; C, c: 60.0 wt%; D, d: 90.0 wt%.

a uniform circular shape. Thus, the inner circle was deformed significantly, seen in Figure 2. However, this situation was impeded when enough NMP was added in the bore fluid, which caused further slower mass transfer and adequate release of centralized stress, shown in Figure 1(C, D). In other words, the initial

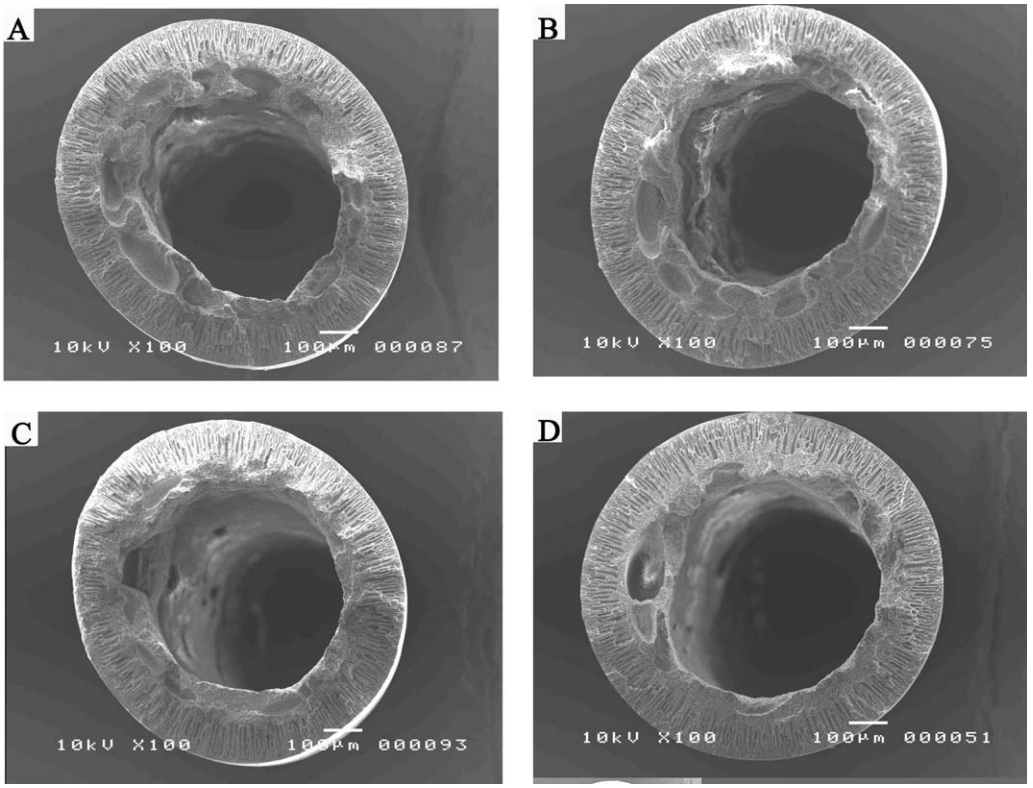

Figure 2 Cross-section of hollow fiber membranes from various bore fluids. Dope flow rate, 12.14 cm^3/min; bore fluid rate, 4.0 cm^3/min; Inner coagulant, NMP aqueous solution. A: 40.0 wt%; B: 45.0 wt%; C: 50.0 wt%; D: 55.0 wt%.

factor of the macrovoid formation were gradually suppressed, finally removed, accordingly, an excellent circle inner surface with macrovoid-free was captured again. For outer surface morphology of the spun fiber, because no effect was imposed under a stable outer operational condition, there was almost no any change observed in this part, seen in Figure 3(A,B).

Santoso et al.[23] also reported irregular inner skin morphology of hollow fiber membranes, but they were generated at high-speed spinning operations. It was hypothesized that this phenomenon occurred due to the formation of vacuum condition in the lumen side of the fiber causing by the rapid formation of dense skin inner layer. Referring to our results shown in Figure 1(A and B), where there was no obvious inner layer deformation though denser inner skins were captured, this proposed mechanism may not be applicable to present cases.

Effect of dope flow rate on the inner surface morphology of the resultant membranes

During the spinning process, it is necessary to keep a sufficiently high viscosity for the dope to ensure the perfect formation of hollow fiber membranes. In such solutions, the macromolecules are usually entangled into conglomerations by physicochemical interactions among the solution components.[24] Therefore, most of the spinning dopes behave like a non-Newtonian fluid.

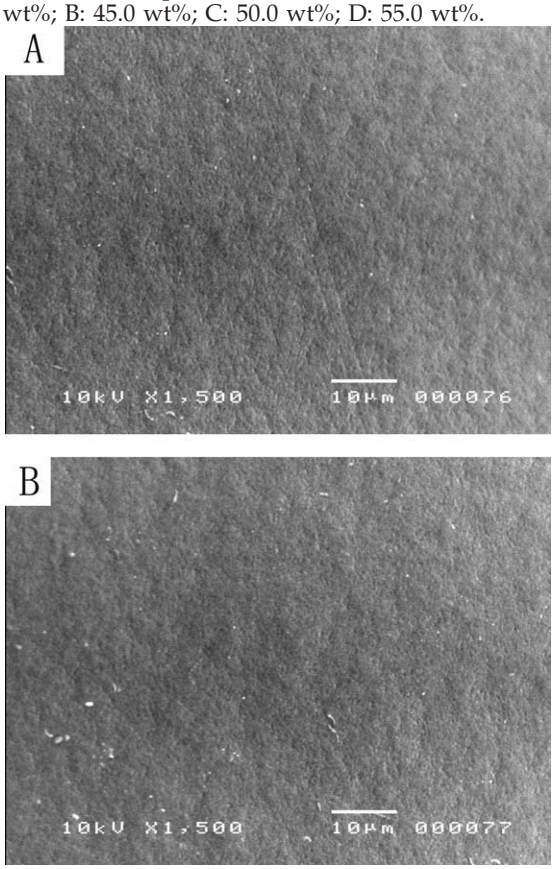

Figure 3 Outer surface morphology of the spun fibers respectively from distilled water and 90 wt % NMP solution as an inner coagulant. A: distilled water; B: 90 wt% NMP solution.

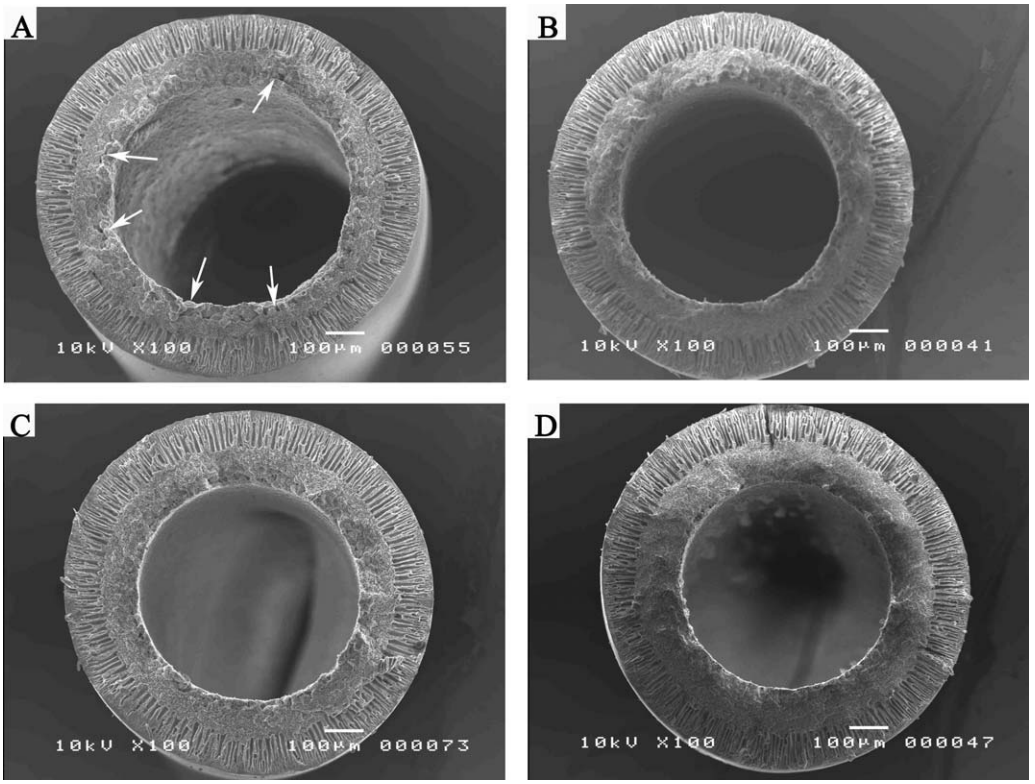

Figure 4 Cross-section of hollow fiber membranes from various dope flow rates. Inner coagulant: 60.0 wt% NMP aqueous solution; dope flow rate A: 4.84 cm^3/min; B: 8.13 cm^3/min; C: 12.14 cm^3/min; D: 21.52 cm^3/min.

In this work, the rheological nature of the model dope was described by the equation: $\tau = 1.482\ \gamma^{0.962}$. Where τ is the shear stress (Pa) and γ is the shear rate (s^{-1}). It indicated that the dope characterized a typical non-Newtonian power-law fluid. When it was subjected to an external force, i.e., a compulsive flow in the spinneret under certain pressure, the macromolecular chain-segments, exactly conglomerations, would be partially orientated.[25]

To evidently reveal the impact of the dope flow on the inner skin structure, a 60.00 wt % NMP aqueous solution as the inner coagulant, and a series of dope flow rates, 4.84, 8.13, 12.14, and 21.52 cm^3/min, were chosen to make hollow fibers, and corresponding morphologies of the resultant membranes are captured in Figure 4, while Table II lists corresponding spinning parameters. It can be seen that some small macrovoids in the margin of the inner skin were visible at the dope rate of 4.84 cm^3/min [Fig. 4(A)], a little illegible at 8.13 cm^3/min [Fig. 4(B)], and almost disappeared at 12.17 cm^3/min and 21.52 cm^3/min [Fig. 4(C,D)]. This can be explained by the rheological behavior of the dope inner layer as it extruded along the spinneret lumen. The macromolecular conglomerations that experienced a higher shear stress tended to align themselves much regular than that underwent a lower shear stress. The macromolecular conglomeration orientation resulted in the formation of a higher strength nascent inner skin than that from a lower spun speed, i.e., the suppression of macrovoids initiation in the inner substructure.

Effect of bore fluid rate on the inner surface morphology of the resultant membranes

Figure 5 exhibits the cross-section morphology of the resultant membranes subjected to various bore fluid rates when a 55.00 wt % NMP aqueous solution was

TABLE II
Spinning Parameters and Fiber Dimensions at Different Dope Flow Rates

Fiber ID	Dope flow rate (cm^3min^{-1})	Bore fluid flow rate (cm^3min^{-1})	Bore fluid composition (NMP/water) (wt/wt)	Outer radius[a] (μm)	Inner radius[a] (μm)	Membrane wall (μm)
No.A	4.84	1.6	60/40	563	346	217
No.B	8.13	2.7	60/40	553	300	253
No.C	12.14	4.0	60/40	561	297	264
No.D	21.52	7.1	60/40	565	312	253

[a] Average outer or inner radius.

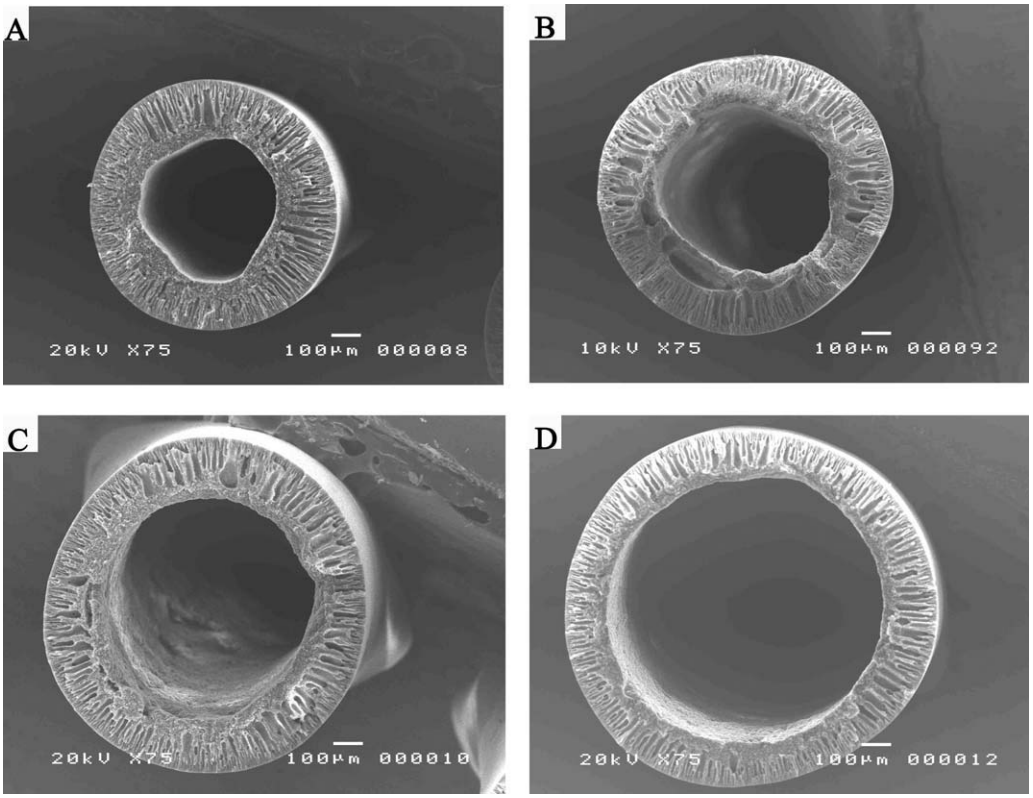

Figure 5 Cross-section of hollow fiber membranes from different inner coagulant rates. Dope flow rate, 12.14 cm^3/min; Inner coagulant, 55.0wt % NMP aqueous solution. A: 2.0 cm^3/min; B: 4.0 cm^3/min; C: 6.0 cm^3/min; D: 8.0 cm^3/min.

used as the bore fluid. It can be seen that the inner layer exhibited a sponge-like structure when the bore fluid rate was small [2.0 cm^3/min; Fig. 5(A)], which is different from the structures formed at a higher bore fluid rate, such as 4.0, 6.0 cm^3/min [Fig. 5(B,C)]. This may be related to the fact that the outflowed NMP from the nascent fiber increased NMP concentration significantly in the bore fluid at a low flow rate, thus lead to a similar situation with these using a high NMP concentration as the bore fluid.

With increase on the bore fluid flow rate, the mass transfer between the solvent and the coagulant in the lumen of fibers was expedited, where the change of the bore fluid composition can be ignored gradually, but the solidification rate at the inner surface increased. When the increase on the solidification rate wasn't high enough, the appearance of macrovoids in the inner sublayer region was evident, as shown in Figure 5(B,C). On the other hand, the increase of the bore fluid rate swelled the inner diameter of the nascent membrane, thinned the membrane wall, which shortens the phase inversion period of the whole membrane matrix. In addition, the outer structure of the membrane was hardly impacted under stable external conditions, i.e., the development of the finger-like pores in the outer sublayer was hardly affected. The two factors made the finger-like pores in the outer sublayer almost transfixed the membrane wall at a high bore fluid rate, seen in Figure 5(D). As a consequence, the development of the macrovoids in the sublayer was suppressed effectively [Fig. 5(C)], even terminated [Fig. 5(D)] at an enough high flow rate.

Performance tests of various membranes for CO_2 capture

To investigate the effect of various fiber structures on the CO_2 capture performance when the membrane

TABLE III
Spinning Conditions and MWCO of Three Experimental Membranes

Fiber ID	Dope flow rate (cm^3min^{-1})	Bore fluid composition (NMP/Water) (wt/wt)	Bore fluid flow rate (cm^3min^{-1})	Water flux ($Lm^{-2}h^{-1}atm^{-1}$)	MWCO
Md	12.14	0/100	4.0	21.7	22,657
M55	12.14	55/45	4.0	30.2	40,455
M90	12.14	90/10	4.0	28.4	45,000

were used as membrane contactors, the membranes made respectively using distilled water (Md), 55.00 wt % (M55) and 90 wt % NMP aqueous solution (M90) as the bore fluid were chosen to represent three different patterns, i.e. double-skin, eliminating inner skin with macrovoids and single-skin, their corresponding structures are shown in Figure1(A), Figure 2(D) and Figure 1(D), while spinning conditions and fiber information are summarized in Table III. It can be seen from Figure 6 that the CO_2 fluxes of all the model membranes increase with accelerated supply of the absorbent, which is in agreement with the accepted behavior from a gas/liquid membrane contactor. The comparison on CO_2 absorption flux under the same absorbent flow velocity indicates an increase tendency in the order of M55>M90>Md.

The three membranes were fabricated under the same spinning conditions except for the bore fluid used. Because the outer quenching bath was fixed in tape water, the phase separation of the outer surface of nascent fibers took place rapidly. It is reasonable to assume that the formation of the fiber outer surface was hardly interfered by the corresponding bore fluid, and thus the three membranes possessed almost the same outer membrane pore structures. This hypothesis can be confirmed indirectly by MWCO of the membranes. It can be seen from Table III that MWCO of M55 and M90 membranes were very close, though Md membrane presented a much smaller MWCO. The difference was attributed to the fact that the dense inner skin layer in Md membrane also played a role in rejecting species. As such, the effect of the membrane outer structure on mass transfer could be approximately deemed to be equal. Consequently, the difference in

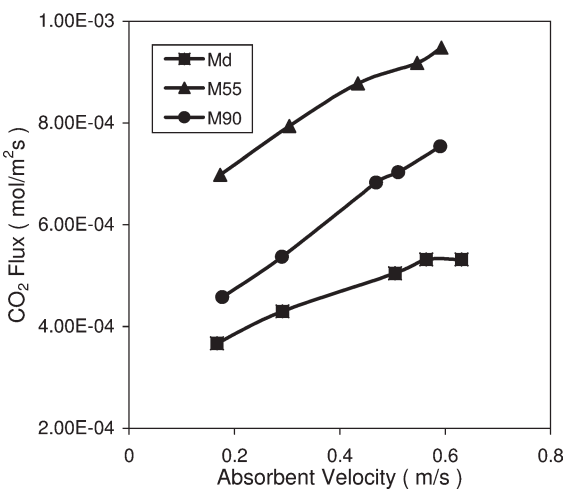

Figure 6 CO_2 absorption flux as a function of absorbent velocity for three model membranes using distilled water saturated by N_2 as an absorbent. The feed CO_2 flow velocity (mol/m^2s): 2.44; operational temperature: 25°C Experimental membrane area (10^{-3} m^2): Md-9.16; M55-9.37; M90-9.29.

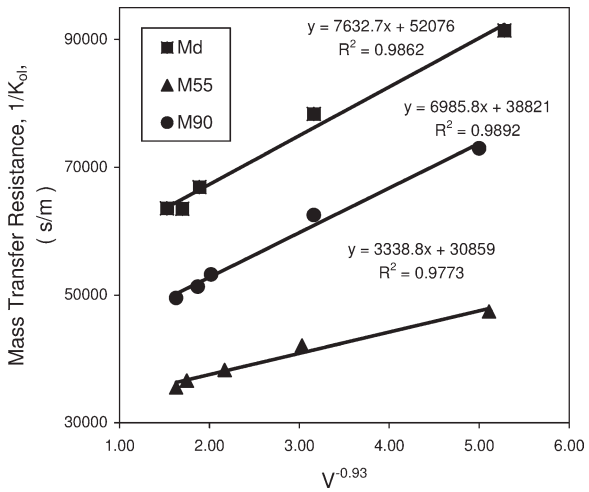

Figure 7 Mass transfer resistance of model membranes vs. $V^{-0.93}$.

CO_2 absorption performance mainly came from the inner structure of the membranes. Referring to the former discussion on the membrane morphology, the elimination of a relative dense inner skin and gradual appearance of a porous inner surface resulted in the decrease of the mass transfer resistance, which were responsible for the increasing tendency on CO_2 flux under the same operating conditions. As shown in Figure 7, the mass transfer resistance of Md membrane was much higher than that of other two membranes. It suggests that the hollow fiber membrane with an inner skin-free layer offers a great advantage on the application as gas/liquid membrane contactors. The similar suggestion was also stated by Aotian et.al.[26] Further inspections on Figures 6 and 7 indicate that M55 membrane represented a relatively higher CO_2 flux and a lower mass transfer resistance than M90 membrane, which may be associated with the existence of macrovoids. In addition, the data on water flux exhibited in Table III also supported the suggestion.

CONCLUSIONS

The morphology development of PVDF hollow fiber membranes subjected to the changes of the bore fluid composition, bore fluid and dope flow rates was investigated in details. It was exhibited that, the morphology of the resultant membranes gradually shifted from a double-skin (0, 20.0 wt % NMP solution) to a single-skin structure (60.0, 90.0 wt.%). However, when 40.0, 45.0, 50.0, 55.00 wt % NMP solutions were respectively used, some macrovoids near the inner region were captured unexpectedly, and with a decrease tendency on macrovoid area along the addition direction of NMP concentration. This special morphology feature was attributed to the reduced solidification rate of the inner surface, which made the inner skin to be weakened.

Although the existence of centralized stress formed in the phase inversion process makes it difficult to maintain a uniform structure. The macrovoids were gradually invisible with increase on the dope flow velocity. Molecular conglomeration orientation was considered to be responsible for the disappearance of the macrovoids. The increase on the bore fluid flow rate also presented impact on the existence of the macrovoids. The elimination of the inner skin effectively reduced the mass transfer resistance of the model membrane, which highlights a potential advantage of hollow fiber membranes with an inner skin-free structure applied in a gas/liquid absorption process as contactors.

NOMENCLATURE

R	correlation coefficient
V	velocity (m s^{-1})

Greek letters

α	constant
τ	shear stress (Pa)
γ	shear rate (s^{-1})

References

1. Zhang, Q.; Cussler, E. L. J Membr Sci 1985, 23, 321.
2. Zhang, Q.; Cussler, E. L. J Membr Sci 1985, 23, 333.
3. Bothum, G. D.; Knutson, B. L.; Strobel, H. J.; Nokes, S. E. J Membr Sci 2003, 227, 183.
4. Dindore, V. Y.; Brilman, D. W. F.; Versteeg, G. F. Chem Eng Sci 2005, 60, 467.
5. Karoor, S.; Sirkar, K. K. Ind Eng Chem Res 1993, 32, 674.
6. Li, J. L.; Chen, B. H. Sep Purif Technol 2005, 41, 109.
7. Wang, R.; Zhang, H. Y.; Feron, P. H. M.; Liang, D. T. Sep Purif Technol 2005, 46, 33.
8. Wang, R.; Li, D. F.; Liang, D. T. Chem Eng Proces 2004, 43, 849.
9. Kim, Y. S.; Yang, S. M. Sep Purif Technol 2000, 21, 101.
10. Kong, J.; Li, K. Sep Purif Technol 1999, 16, 83.
11. Khayet, M.; Feng, C. Y.; Khulbe, K. C.; Matsuura, T. Desalination 2002, 148, 321.
12. Wang, D.; Li, K.; Teo, W. K. J Membr Sci 1999, 163, 211.
13. Ren, J. Z.; Wang, R.; Zhang, H. Y.; Li, Z. S.; Liang, D.; Tay, J. J Membr Sci 2006, 261, 334.
14. Wijmans, J. G.; Baaij, J. P. B.; Smolders, C. A. J Membr Sci 1983, 14, 263.
15. Wijmans, J. G.; Kant, J.; Mulder, M. H. V.; Smolders, C. A. Polymer 1985, 26, 1539.
16. Fujii, Y.; Kigoshi, S.; Iwatani, H.; Aoyama, M. J Membr Sci 1992, 72, 53.
17. Deshmukh, S. P.; Li, K. J Membr Sci 1998, 150, 75.
18. Kayet, M.; Feng, C. Y.; Khulbe, K. C.; Matsuura, T. Polymer 2002, 43, 3879.
19. Zhang, H. Y.; Wang, R.; Liang, D. T.; Tay, J. J Membr Sci 2006, 279, 301.
20. Atchariyawut, S.; Feng, C. S.; Wang, R.; Jiraratananon, R.; Liang, D. T. J Membr Sci 2006, 285, 272.
21. Strathmann, H.; Kock, K.; Amar, P.; Baker, R. W. Desalination 1975, 16, 179.
22. Strathmann, H. ACS Symp Ser 1985, 26, 165.
23. Santoso, Y. E.; Chung, T. S.; Wang, K. Y.; Weber, M. J Membr Sci 2006, 282, 383.
24. He, M. J.; Dong, X. X. Polymer Physics; Fudan University Press: Shanghai, 1990; p 114.
25. Qin, J. J.; Chung, T. S. J Membr Sci 1999, 157, 35.
26. Xu, A. T.; Yang, A. H.; Young, S.; David, D.; Paitoon, T. J Membr Sci 2008, 311, 153.